Global optical potential for ^{7}Be on various targets at sub- and near-barrier energies

Athena Pakou *
Department of Physics and HINP, The University of Ioannina, 45110 Ioannina, Greece

(Received 2 October 2023; accepted 7 December 2023; published 9 January 2024)

A global phenomenological energy dependent optical potential for the radioactive nucleus ^{7}Be on various targets is developed. This optical potential is based on Woods-Saxon form factors with a smooth mass dependent potential depth for above-barrier energies and an energy and mass dependent depth below barrier. The potential is validated with elastic scattering and fusion calculations which are compared with experimental data and are found to be in very good agreement. The present potential is compared with the energy dependent Cook potential, developed for ^{6}Li and ^{7}Li.

DOI: 10.1103/PhysRevC.109.014609

I. INTRODUCTION

Weakly bound nuclei, either radioactive or stable, attract the interest of physicists as open quantum systems, due to their strong interactions with the continuum environment. This may lead to unexpected phenomena in elastic scattering as well as to large enhancements in sub-barrier fusion. Good examples in that direction are the ^{11}Li and ^{11}Be nuclei, where a dramatic deviation from Rutherford scattering below barrier occurs for the first one and a strong rainbow suppression for the second one [1–3] at sub- or near-barrier energies. Such effects are produced via Coulomb and/or nuclear couplings to continuum, interpreted via Continuum Discretized Coupled Channel (CDCC) calculations. Another interesting case is the behavior of the proton halo nucleus ^{8}B. In contrast to the above neutron rich nuclei, no dramatic coupled channel effects are observed and only slight deviations occur between uncoupled and CDCC calculations, despite the large measured breakup cross sections [4–7]. These large cross sections persist up to very deep sub-barrier energies, where the distance of closest approach is several times the sum of radii of the colliding nuclei and the breakup probability is rather of pure Coulomb type [5].

Generally speaking, CDCC calculations taking into account continuum excitations or coupled reaction channels (CRC) calculations taking into account transfer channels require input potentials which have to be sought from the literature [8–14]. Such potentials are of critical importance for the success of the calculation and the interpretation of measurements with weakly bound nuclei, especially at sub- and near-barrier energies. For ^{8}B on various targets one of the needed input potentials is the potential of the breakup fragment ^{7}Be with the specific target. In this respect, it is of primary importance to obtain a global potential with ^{7}Be as projectile on various targets. Underlined here is the necessity of an energy dependent potential at low energies, where the existence of the threshold potential anomaly (TA) [15–18] is well established. This anomaly for well bound nuclei is described through a dispersion relation which connects the decrease of the imaginary part of the potential when approaching the Coulomb barrier from higher to lower energies with the real part of the potential, which appears at the barrier as a bell shaped peak. For weakly bound nuclei, however, with emphasis on research with the weakly bound but stable ^{6}Li and ^{7}Li nuclei, the energy dependence of the potential presents conflicting results [19–21]. Variations occur not only between ^{6}Li and ^{7}Li but also between collisions either with light or with heavy targets [22]. For ^{7}Li and ^{7}Be, the energy dependence of the optical potential resembles that of well bound nuclei, with the appearance of the standard TA. But this is valid only for the heavier targets. It was reported recently [22,23] that for lighter targets like ^{28}Si the real part of the potential is flat and constant, while the transition between a flat potential and a bell shaped one occurs for targets with mass numbers close to that of ^{90}Zr [23]. It was also shown that the potential for ^{7}Be resembles that of ^{7}Li for both light and heavy targets [22,24]. This contradicts the fact that the breakup threshold for ^{7}Be is 1.59 MeV, close to the threshold of ^{6}Li, 1.47 MeV, and not that of its mirror nucleus ^{7}Li, 2.37 MeV. Within this context, the development of a global energy dependent optical potential for ^{7}Be should take into account the above issues and can be validated in a consistent analysis of ^{7}Be scattering and fusion on a variety of targets. This would answer the fundamental question posed in Ref. [25] by Keeley, Kemper, and Rusek, as to whether the elastic scattering and fusion of weakly bound nuclei is governed by their breakup threshold, in which case the behavior of ^{7}Be will follow that of ^{6}Li, or by their internal structure, and then ^{7}Be and ^{7}Li will behave the same.

^{7}Be is a very challenging nucleus, involved in the yet unresolved cosmological lithium problem [26] regarding the discrepancy between the measurement and the big bang nucleosynthesis (BBN) predicted abundance. In BBN, it is produced via ^{7}Be. Its production [^{3}He$(\alpha,\gamma)^{7}$Be] and destruction [^{7}Be$(n,\alpha)^{4}$He and ^{7}Be$(n,p)^{7}$Li] are of critical importance [27–30], and any information related to this nucleus, including

*apakou@uoi.gr

 ©2024 American Physical Society

the potentials, should be important. Several global potentials for ^{6}Li and ^{7}Li were developed in the past [31–33] and are evaluated for various systems in Ref. [34]. In the same reference the imaginary part of the Cook potential [31] was modified to include the energy dependence. Therefore, it will be interesting to make the appropriate comparisons with the modified Cook potential either for ^{6}Li and/or for ^{7}Li and propose a global optical potential to be used for predicting reaction observables in regions where no measurements exist.

Presented in Sec. II is the potential and the validation via elastic scattering and fusion calculations, in comparison with experimental data. Then, in Sec. III, the results are discussed and the final conclusions are given.

II. THE POTENTIAL

The potential is assumed to have a Woods-Saxon form with a smooth mass dependent depth at above-barrier energies, and an energy and mass dependent depth at below-barrier energies.

In more detail the depth of the real part of the potential at above-barrier energies for targets with $A = 28$ to 208 is parametrized as

$$V = 0.0006027A^2 + 3.034A - 11.69 \text{ MeV}. \quad (1)$$

At below-barrier energies the same relation can be used for targets with mass numbers $28 < A < 90$. For heavier targets $A = 90$ to $A = 208$ the following relation as a function of energy should apply:

$$V/A = 3.703(E/V_B)^{-2.0865} \text{ MeV}. \quad (2)$$

For the imaginary part and for all targets, the potential above barrier is taken to be energy independent and can be written as

$$W = 0.9666A + 56.93 \text{ MeV} \quad (3)$$

Below barrier an energy dependence is necessary and the potential can be either written as

$$W/A = 9.45126(E/V_B)^2 - 15.578(E/V_B) \text{ MeV}, \quad (4)$$

or for $E/V_B > 0.86$ as

$$W/A = 1.25(E/V_B) - 0.305 \text{ MeV}, \quad (5)$$

and for $E/V_B < 0.86$ as

$$W/A = 0.767 \text{ MeV}, \quad (6)$$

where A is the mass number, E the projectile energy in the center of mass, and V_B the Coulomb barrier according to Broglia [35], as appears in the following equation in the center of mass, expressed in MeV:

$$V_B = \frac{R_f \times 1.44 Z_1 Z_2}{R_2} \quad (7)$$

with

$$R_f = 1 - \frac{0.63}{R_2} \quad (8)$$

and

$$R_2 = \left[1.07\left(A_1^{1/3} + A_2^{1/3}\right) + 2.72\right] \text{fm}, \quad (9)$$

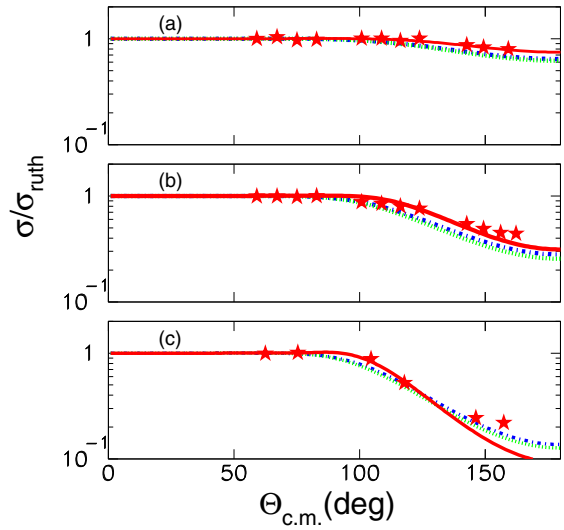

FIG. 1. Previous angular distribution data for ^{7}Be + ^{208}Pb, at (a) 37.6 MeV, (b) 40.5 MeV, (c) 42 MeV, are compared with OMP calculations. Calculations with the present potential are designated with the solid red line, while those with the Cook potential for ^{7}Li and ^{6}Li are shown with the dashed green and dotted-dashed blue lines, respectively. The data are from Ref. [36].

where Z_1, Z_2, A_1, A_2, are the atomic and mass numbers of projectile and target, respectively.

For all energy regions the geometrical parameters of the Woods-Saxon form factor are taken for the reduced radii and diffusivities respectively as

$$r_0^r = 0.815 \text{ fm} \quad \text{and} \quad r_0^i = 0.83 \text{ fm} \quad (10)$$

and

$$a^r = a^i = 0.855 \text{ fm} \quad (11)$$

with the radii given as $R = r_0(A_1^{1/3} + A_2^{1/3})$ fm.

Underlined here is the constant step in the imaginary potential, described by Eq. (6) at energies below $E/V_B = 0.86$. The possible existence of such a step was verified in studies with ^{7}Li [39] and studies with ^{7}Be [24]. It will be very interesting to see further research in this direction, delineating the energy regime of this constant loss of flux from the elastic channel and the related reaction mechanism.

A. Elastic scattering

The potential described above was used to calculate elastic scattering angular distributions for ^{7}Be on various targets such as ^{208}Pb, ^{90}Zr, ^{58}Ni, and ^{28}Si, displayed in Figs. 1–4, respectively. These calculations are compared with existing data [23,24,36–38]. As can be seen, the agreement is very good. Then the calculations are repeated with the modified Cook potential [34] and the results are also included in the same figures. Taking into account that this potential was extracted for lithium projectiles, the agreement is adequately good, although not equally as good as with the present potential. Further on, another interesting point will be underlined, re-

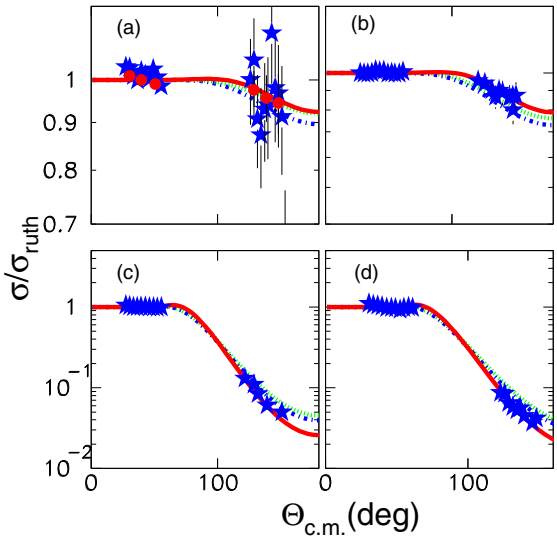

FIG. 2. Previous angular distribution data for ^{7}Be + ^{90}Zr, at (a) 19.7 MeV, (b) 21.3 MeV, (c) 27.1 MeV, (d) 27.5 MeV, are compared with OMP calculations. Calculations with the present potential are designated with the solid red line, while those with the Cook potential for ^{7}Li and ^{6}Li are shown with the dashed green and dotted-dashed blue lines respectively. The data are from Ref. [23]. Note that the data at 26.6 MeV now appear as data at 27.1 MeV due to a recalibration of the beam energies.

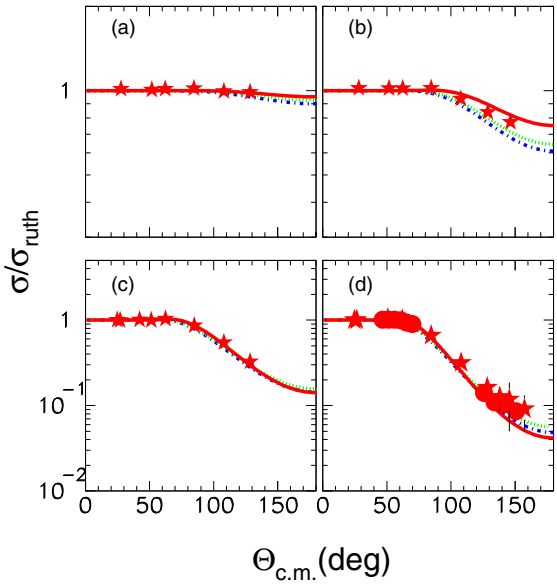

FIG. 3. Previous angular distribution data for ^{7}Be + ^{58}Ni, at (a) 15.1 MeV, (b) 17.1 MeV, (c) 19.9 MeV, (d) 21.5 MeV, are compared with OMP calculations. Calculations with the present potential are designated with the solid red line, while those with the Cook potential for ^{7}Li and ^{6}Li are shown with the dashed green and dotted-dashed blue lines, respectively. The data designated with the stars are from Ref. [37] for all energies, while for the highest energy data of Ref. [38] also appear and are designated with the filled circles.

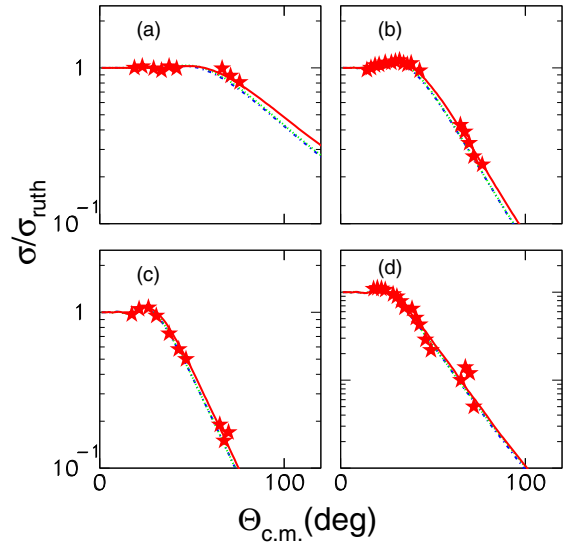

FIG. 4. Previous angular distribution data for ^{7}Be + ^{28}Si, at (a) 12.9 MeV, (b) 16.7 MeV, (c) 19.5 MeV, (d) 21.7 MeV, are compared with OMP calculations. Calculations with the present potential are designated with the solid red line, while those with the Cook potential for ^{7}Li and ^{6}Li are shown with the dashed-green and dotted-dashed blue lines, respectively. The data are from Ref. [24].

lated to a nonsubstantial differentiation between calculations with the ^{7}Li or the ^{6}Li modified Cook potential.

Next is an attempt to compare calculations with the present potential and the modified ^{6,7}Li Cook potential for ^{7}Li elastic scattering on various targets, where previous data exist. These targets are ^{208}Pb, ^{144}Sm, ^{138}Ba, ^{64}Zn, ^{58}Ni, and ^{28}Si at various sub- and near-barrier energies. The results are presented in Figs. 5–10, respectively, for the above targets. The comparison

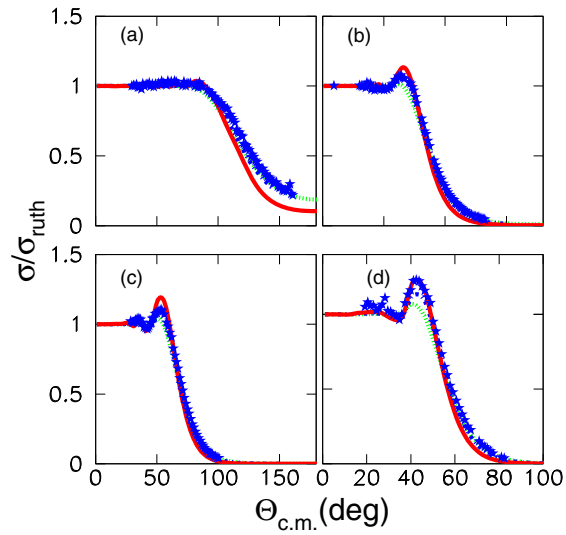

FIG. 5. Previous angular distribution data for ^{7}Li + ^{208}Pb, at (a) 31 MeV, (b) 35 MeV, (c) 39 MeV, (d) 44 MeV, are compared with OMP calculations. Calculations with the present potential are designated with the solid red line, while those with the Cook potential for ^{7}Li and ^{6}Li are shown with the dashed green and dotted-dashed blue lines, respectively. The data are from Ref. [39].

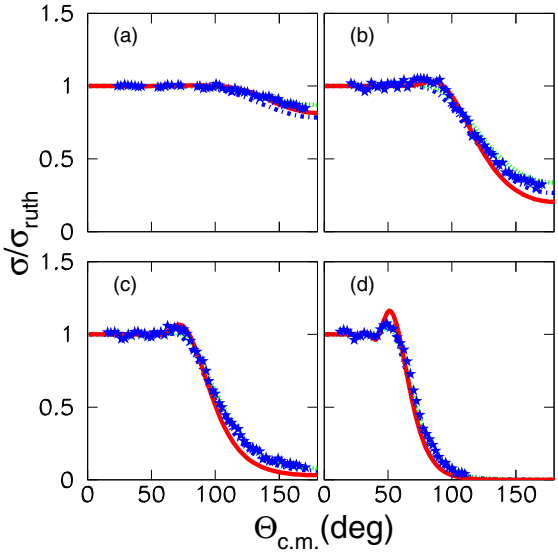

FIG. 6. Previous angular distribution data for ^{7}Li + ^{144}Sm, at (a) 22.6 MeV, (b) 25 MeV, (c) 27 MeV, (d) 32 MeV, are compared with OMP calculations. Calculations with the present potential are designated with the solid red line, while those with the Cook potential for ^{7}Li and ^{6}Li are shown with the dashed green and dotted-dashed blue lines, respectively. The data are from Ref. [40].

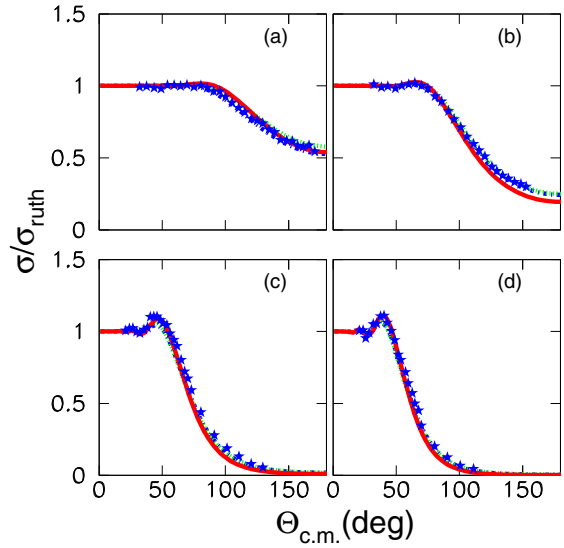

FIG. 8. Previous angular distribution data for ^{7}Li + ^{64}Zn, at (a) 23.8 MeV, (b) 15.02 MeV, (c) 18.15 MeV, (d) 20.12 MeV, are compared with OMP calculations. Calculations with the present potential are designated with the solid red line, while those with the Cook potential for ^{7}Li and ^{6}Li are shown with the dashed green and dotted-dashed blue lines, respectively. The data are from Ref. [42].

of data and calculations with the present potential is fair. While the data are reproduced very well for forward angles, at backward angles the agreement is not equally good. The results with the Cook potential referring either to ^{6}Li or to ^{7}Li are very good. On the other hand, a better agreement at the rainbow region for the higher energies is obtained with the present potential. This is displayed in Fig. 11, where the rainbow structure is clearly observed for three systems, ^{7}Li on ^{208}Pb, ^{144}Sm, and ^{138}Ba at 52 MeV. Finally, in Fig. 12, calculations with the modified Cook potential and the present one for ^{6}Li + ^{90}Zr are compared with previous data [48]. As expected for the sub- barrier energies, where the energy dependence of the optical potential for ^{6}Li is very different

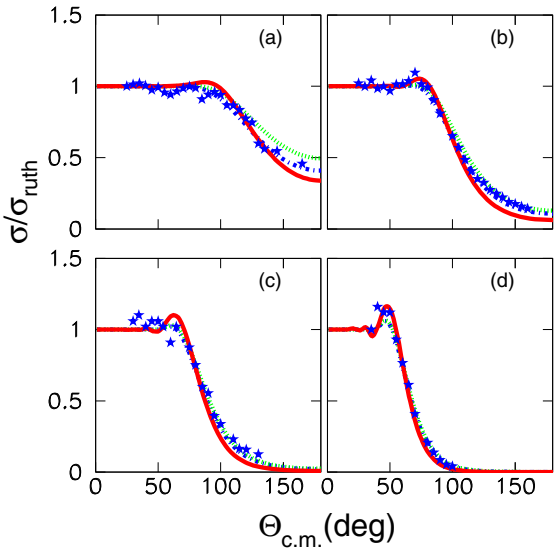

FIG. 7. Previous angular distribution data for ^{7}Li + ^{138}Ba, at (a) 22. MeV, (b) 24 MeV, (c) 26 MeV, (d) 30 MeV, are compared with OMP calculations. Calculations with the present potential are designated with the solid red line, while those with the Cook potential for ^{7}Li and ^{6}Li are shown with the dashed green and dotted-dashed blue lines, respectively. The data are from Ref. [41].

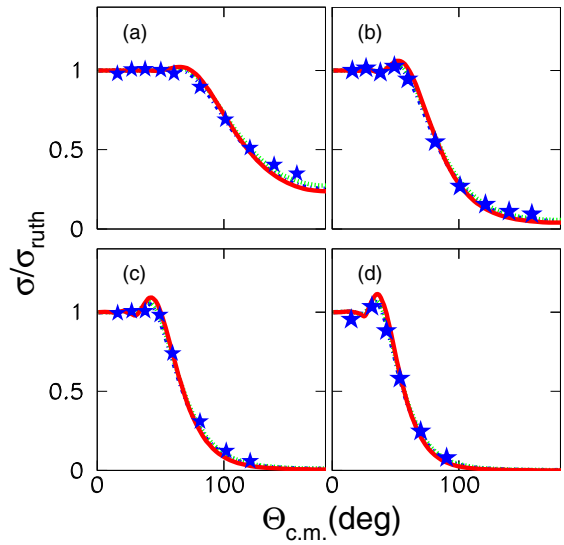

FIG. 9. Previous angular distribution data for ^{7}Li + ^{58}Ni, at (a) 14.22 MeV, (b) 16.25 MeV, (c) 18.28 MeV, (d) 20.31 MeV, are compared with OMP calculations. Calculations with the present potential are designated with the solid red line, while those with the Cook potential for ^{7}Li and ^{6}Li are showm with the dashed-green and dotted-dashed blue lines, respectively. The data are from Ref. [43].

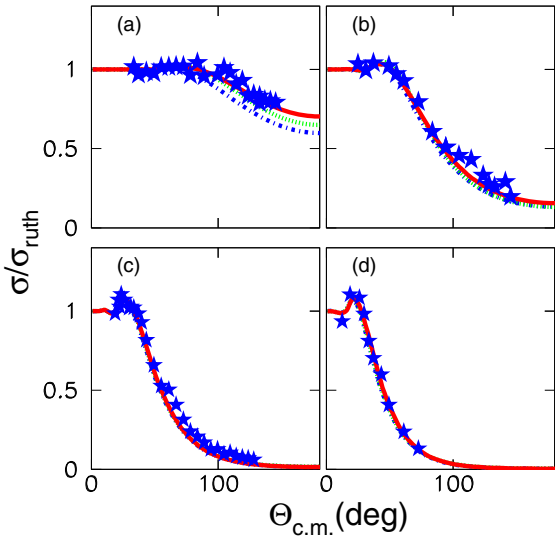

FIG. 10. Previous angular distribution data for ^{7}Li + ^{28}Si, at (a) 7.8 MeV, (b) 9.82 MeV, (c) 12.84 MeV, (d) 14.85 MeV, are compared with OMP calculations. Calculations with the present potential are designated with the solid red line, while those with the Cook potential for ^{7}Li and ^{6}Li are shown with the dashed- green and dotted-dashed blue lines, respectively. The data are from Ref. [44].

from that of ^{7}Li and ^{7}Be, the agreement with data is very good only for the modified Cook potential for ^{6}Li. At higher energies calculations with all the potentials deviate from data at backward angles.

Described above are the validation of the suggested potential versus the modified Cook one [34], taking into account elastic scattering data. In the next subsection the validity of these potentials will be further explored with fusion one-BPM calculations.

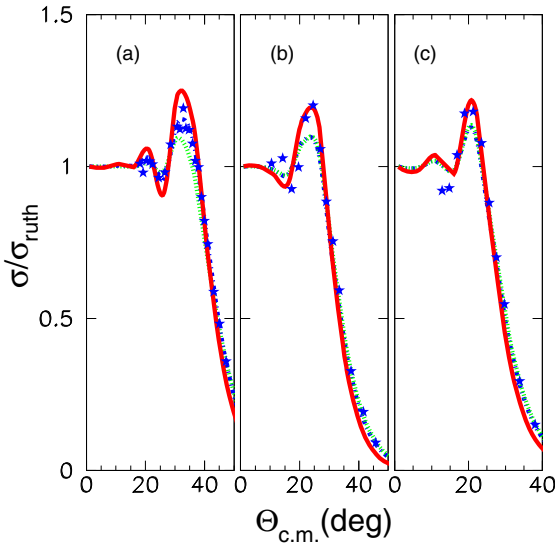

FIG. 11. Elastic scattering data at 52 MeV for (a) ^{7}Li + ^{208}Pb [45], (b) ^{7}Li + ^{144}Sm [46], and (c) ^{7}Li + ^{138}Ba [47], are compared with calculations adopting the present potential, solid red line, and the ^{6,7}Li modified Cook potential, designated with the dotted dashed and dashed blue and green lines. The rainbow structure is clearly seen and it is reproduced very well with the present potential.

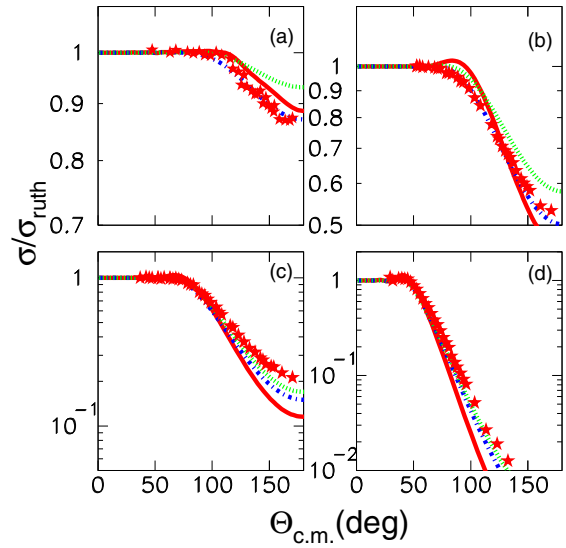

FIG. 12. Previous angular distribution data for ^{6}Li + ^{90}Zr, at (a) 14.89 MeV, (b) 16.9 MeV, (c) 18.9 MeV, (d) 24.92 MeV, are compared with OMP calculations. Calculations with the present potential are designated with the solid red line, while those with the Cook potential for ^{7}Li and ^{6}Li are shown with the dashed green and dotted-dashed blue lines, respectively. The data are from Ref. [48].

B. Fusion excitation functions

Barrier Penetration Model (BPM) calculations were performed with the code ECIS [49–51] for the ^{7}Be + ^{208}Pb system, taking into account the present potential and the modified Cook potential for ^{6,7}Li. The results, appropriately reduced, are compared with two series of data for ^{7}Li + ^{209}Bi and ^{9}Be + ^{208}Pb, due to lack of ^{7}Be fusion data. Experimental data and calculations are appropriately reduced as follows, according to Ref. [53]:

$$\sigma_F \rightarrow F(x) = \frac{2E_{\text{c.m.}}}{\hbar\omega R_B^2}\sigma_F \tag{12}$$

corresponding to an energy $E_{\text{c.m.}}$ of the projectile reduced to the quantity x given by the equation

$$E_{\text{c.m.}} \rightarrow x = \frac{E_{\text{c.m.}} - V_B}{\hbar\omega}. \tag{13}$$

The reduced quantity $F(x)$ is traditionally compared with the so-called universal fusion function (UFF), corresponding to the Wong fusion cross section σ_W in the one-barrier penetration model [52],

$$\sigma_W \rightarrow F_0(x) = \frac{2E_{\text{c.m.}}}{\hbar\omega R_B^2}\sigma_W = \ln[1 + e^{(2\pi x)}]. \tag{14}$$

The parameters of the Wong potential [52] used for the reduction, namely the curvature $\hbar\omega$, the barrier V_B, and the radius R_B, are included in Table I. The results are displayed in Fig. 13. It can be seen that calculations with the present potential predict a fusion enhancement below barrier, as they

TABLE I. Parameters used for the reduction of the fusion cross sections.

System	$\hbar\omega$ (MeV)	V_B (MeV)	R_B (fm)
^{9}Be + ^{208}Pb	4.704	39.174	11.351
^{7}Li + ^{209}Bi	4.721	30.091	11.215
^{7}Be + ^{208}Pb	5.413	40.111	11.066
^{7}Be + ^{90}Zr	4.555	22.69	9.447
^{7}Be + ^{58}Ni	4.193	17.047	8.756
^{7}Be + ^{28}Si	3.481	9.351	7.92
^{6}Li + ^{59}Co	3.837	12.251	8.822
^{6}Li + ^{120}Sn	4.507	20.287	9.948

should, but not to the extent of the "exact" calculation with the BDM3Y1 interaction reported in Ref. [22]. On the other hand the predictions with the Cook potential are not satisfactory as they remain lower than or equal to the uncoupled prediction of Wong cross sections (UFF curve). Similar calculations for ^{6}Li + ^{90}Zr are plotted against data on ^{59}Co and ^{120}Sn targets in Fig. 14. Even in that case, only the present potential is capable of producing some enhancement, but not adequately to describe the data. Subsequently the present calculations for ^{7}Be on all targets (^{208}Pb, ^{90}Zr, ^{58}Ni, ^{28}Si) with the three potentials are presented in Fig. 15. It is again obvious that only with the present potential can a fusion enhancement be predicted. The results will be commented on below.

III. DISCUSSION AND CONCLUSIONS

Suggested in this work is an energy and target mass dependent algorithm for describing the optical potential for ^{7}Be on various light, medium and heavy targets at sub- and near-barrier energies. Overall, this potential can adequately reproduce both elastic scattering and fusion cross sections. The same algorithm can be used for predicting elastic and fusion cross sections for ^{7}Li projectiles on various targets. In that case, however, the prediction of elastic scattering at backward angles is fair. At the most forward angles and above-barrier energies, the rainbow formation can be very well reproduced. Results for elastic scattering of ^{6}Li are not reproducible within the present model.

The effect of the present potential on elastic scattering and on fusion versus the Cook potential [31] in its recent energy dependent formalism [34] was also considered. The Cook potential can fairly well describe the elastic scattering

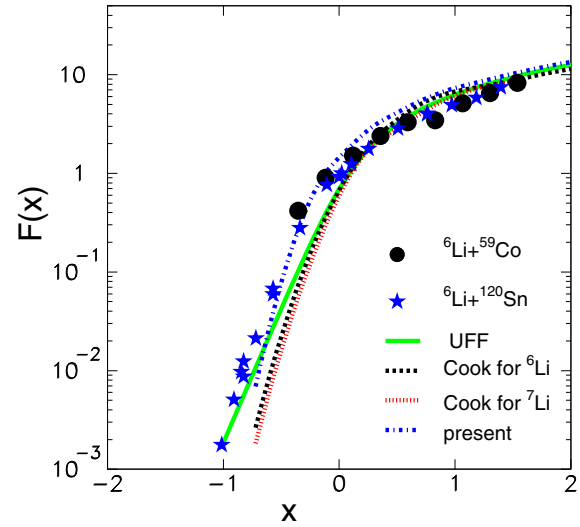

FIG. 14. Barrier penetration fusion calculations, appropriately reduced, are presented for ^{6}Li + ^{90}Zr with the present potential and the ^{6}Li and ^{7}Li Cook ones. The calculations are compared with total fusion data [55,56] for ^{59}Co and ^{120}Sn due to lack of data on ^{90}Zr.

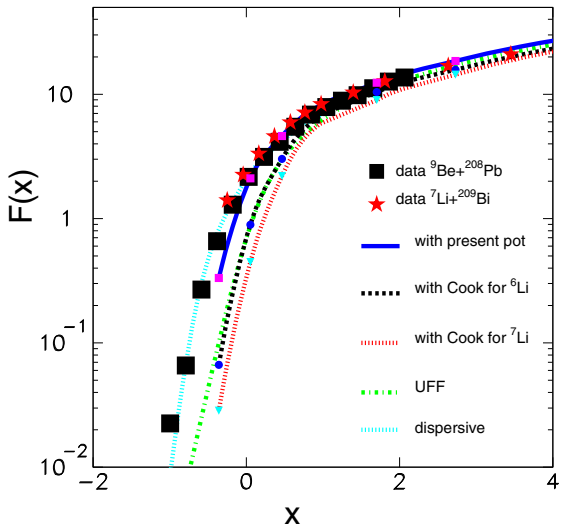

FIG. 13. Previous fusion data for ^{9}Be + ^{208}Pb and ^{7}Li + ^{209}Bi [54] are compared with BPM calculations taking into account a dispersion corrected potential [22], the present potential, the modified Cook potential for ^{6,7}Li, and the Wong prediction (UFF).

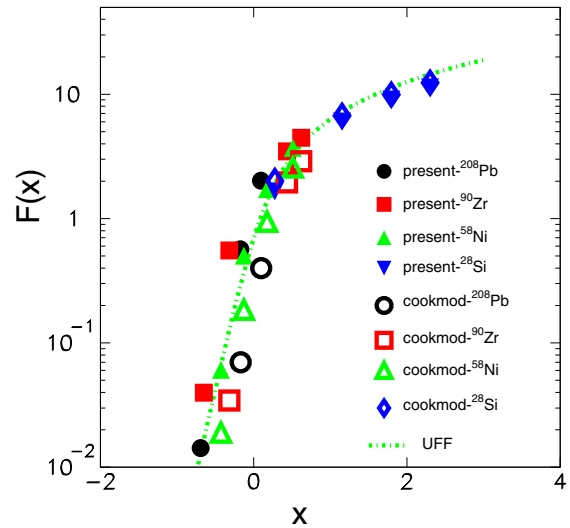

FIG. 15. Barrier penetration fusion calculations, appropriately reduced, are presented for light, medium, and heavy mass targets with the present potential as well as with the modified Cook potential for ^{6,7}Li, for ^{7}Be on various targets as shown in the inset.

of ^{7}Be on various targets and very well describe ^{7}Li elastic scattering data at this sub- and near-barrier energy region. It should be noted that both Cook potentials for ^{6}Li and ^{7}Li present almost identical behavior. For the case of ^{6}Li, the only potential which can describe elastic scattering data is the Cook one for ^{6}Li and not the Cook one for ^{7}Li or the present one for ^{7}Be. Further on, commenting on the present results on fusion, the present potential can predict a substantial enhancement below barrier for the heavier targets and no enhancement for the light ones. The Cook potential in either form for ^{7}Li or for ^{6}Li can reproduce any enhancement, occasionally predicting fusion cross sections even below the Wong prediction.

In more detail, an inspection of Fig. 15 reveals the following interesting issues. As already seen from Fig. 13 for heavy targets, the present potential is superior to the Cook one as it gives fusion enhancement versus the UFF curve. For lighter targets, the calculated fusion cross sections come closer to the Wong calculations or coincide with it. This is expected since for heavy targets a dispersive correction to the real part of the potential represents strong coupled channel effects realized with a fusion enhancement below barrier. For lighter targets couplings to direct channels are weak, the potential becomes flat, and a weak or no fusion enhancement is expected to be observed. For the Cook potential for all targets, calculations are kept around the Wong prediction, failing to predict any enhancement below barrier. This becomes evident if one compares the present real part of the potential with the BDM3Y1 interaction and the Cook potential; see Fig. 16. Indeed the depths of the potential in the interior are different for the present and the Cook potentials. The present potential is similar to the BDM3Y1 interaction, but still less deep. It should be noted here that the modification in the Cook potential is only related to the imaginary part and therefore is irrelevant in the present fusion calculation in a one-BPM model.

In summary

(i) The present optical potential can very well reproduce elastic scattering and fusion cross sections at sub- and near-barrier energies for ^{7}Be projectiles on light, medium, and heavy targets. It can fairly well reproduce elastic scattering and fusion of ^{7}Li on the same targets. It can not predict elastic scattering for ^{6}Li projectiles

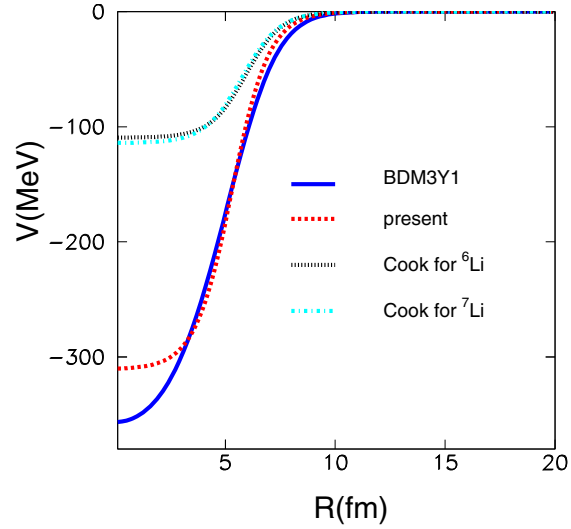

FIG. 16. The present optical potential is compared with the modified Cook potential for ^{6,7}Li and a BDM3Y1 interaction for the system ^{7}Be + ^{90}Zr at projectile energy of 27 MeV.

(ii) The modified Cook potential for both the ^{6}Li or ^{7}Li formalisms can very well reproduce the sub- and near-barrier elastic scattering data for ^{7}Li and fairly well reproduce the ^{7}Be elastic scattering. Elastic scattering data for ^{6}Li can be represented only by the Cook ^{6}Li algorithm

(iii) The Cook potential cannot reproduce any fusion enhancement below barrier for any projectile and target combination.

From the above, it can be concluded that the present optical potential is a global potential capable of predicting elastic scattering and fusion below and near barrier very well for ^{7}Be on various targets ($A = 28$ to 208) and fairly well for its mirror ^{7}Li. This potential was validated only for energies in the sub- and near-barrier region.

ACKNOWLEDGMENTS

I warmly acknowledge the contribution in this work of K. Palli, O. Sgouros, V. Soukeras, and Prof. George Souliotis by carefully reading the manuscript.

[1] M. Cubero *et al.*, Phys. Rev. Lett. **109**, 262701 (2012).
[2] A. Di Pietro *et al.*, Phys. Rev. Lett. **105**, 022701 (2010).
[3] N. Keeley, N. Alamanos, K. W. Kemper, and K. Rusek, Phys. Rev. C **82**, 034606 (2010).
[4] N. Keeley, N. Alamanos, K. W. Kemper, and K. Rusek, Prog. Part. Nucl. Phys. **63**, 396 (2009).
[5] A. Pakou *et al.*, Phys. Rev. C **102**, 031601(R) (2020).
[6] R. Spartà *et al.*, Phys. Lett. B **820**, 136477 (2021).
[7] L. Yang *et al.*, Nat. Commun. **13**, 7193 (2022).
[8] F. Nunes, Scholarpedia **6**, 10497 (2011).
[9] R. C. Johnson and R. J. R. Soper, Phys. Rev. C **1**, 976 (1970).
[10] G. Rawitscher, Phys. Rev. C **9**, 2210 (1974).
[11] K. Rusek, N. M. Clarke, and R. P. Ward, Phys. Rev. C **50**, 2010 (1994).
[12] K. Rusek, P. V. Green, P. L. Kerr, and K. W. Kemper, Phys. Rev. C **56**, 1895 (1997).
[13] I. J. Thompson, Comput. Phys. Rep. **7**, 167 (1988).
[14] K. Hagino, K. Ogata, and A. M. Moro, Prog. Part. Nucl. Phys. **125**, 103951 (2022).
[15] G. R. Satchler, Phys. Rep. **199**, 147 (1991).
[16] C. Mahaux, H. Ngo, and G. R. Satchler, Nucl. Phys. A **449**, 354 (1986).
[17] M. A. Nagarajan, C. C. Mahaux, and G. R. Satchler, Phys. Rev. Lett. **54**, 1136 (1985).

[18] M. A. Nagarajan and G. R. Satchler, Phys. Lett. B **173**, 29 (1986).
[19] P. R. S. Gomes, J. Lubian, L. F. Canto, D. R. Otomar, D. R. Mendes Junior, P. N. de Faria, R. Linares, L. Sigaud, J. Rangel, J. L. Ferreira *et al.*, Few Body Syst. **57**, 165 (2016).
[20] L. F. Canto, P. R. S. Gomes, R. Donangelo, and M. S. Hussein, Phys. Rep. **424**, 1 (2006).
[21] A. Pakou, O. Sgouros, V. Soukeras, and F. Cappuzzello, Eur. Phys. J. A **58**, 8 (2022).
[22] O. Sgouros, V. Soukeras, K. Palli, and A. Pakou, Phys. Rev. C **106**, 044612 (2022).
[23] K. Palli *et al.*, Phys. Rev. C **107**, 064613 (2023).
[24] O. Sgouros *et al.*, Phys. Rev. C **95**, 054609 (2017).
[25] N. Keeley, K. W. Kemper, and K. Rusek, Phys. Rev. C **66**, 044605 (2002).
[26] R. H. Cyburt, B. D. Fields, K. A. Olive, and T.-H. Yeh, Rev. Mod. Phys. **88**, 015004 (2016).
[27] P. E. Koehler *et al.*, Phys. Rev. C **37**, 917 (1988).
[28] M. Barbagallo *et al.*, Phys. Rev. Lett. **117**, 152701 (2016).
[29] L. Lamia *et al.*, Astrophys. J. **850**, 175 (2017).
[30] E. M. Tursunov, S. A. Turakulov, and A. S. Kadyrov, Nucl. Phys. A **1006**, 122108 (2021).
[31] J. Cook, Nucl. Phys. A **388**, 153 (1982).
[32] Y. Xu, Y. Han, J. Hu, H. Liang, Z. Wu, H. Guo, and C. Cai, Phys. Rev. C **97**, 014615 (2018).
[33] Y. Xu, Y. Han, J. Hu, H. Liang, Z. Wu, H. Guo, and C. Cai, Phys. Rev. C **98**, 024619 (2018).
[34] V. A. B. Zagatto, B. R. Goncalves, and D. R. Mendes Junior, Phys. Rev. C **107**, 044604 (2023).
[35] R. A. Broglia and A. Winther, *Heavy Ion Reactions, Volume I: Elastic and Inelastic Reactions* (Benjamin/Cummings, San Francisco, 1981).
[36] M. Mazzocco *et al.*, Phys. Rev. C **100**, 024602 (2019).
[37] E. F. Aguilera, E. Martinez-Quiroz, D. Lizcano, A. Gomez-Camacho, J. J. Kolata, L. O. Lamm, V. Guimaraes, R. Lichtenthaler, O. Camargo, F. D. Becchetti, H. Jiang, P. A. DeYoung, P. J. Mears, and T. L. Belyaeva, Phys. Rev. C **79**, 021601(R) (2009).
[38] M. Mazzocco *et al.*, Phys. Rev. C **92**, 024615 (2015).
[39] N. Keeley, S. J. Bennett, N. M. Clarke, B. R. Fulton, G. Tungate, P. V. Drumm, M. A. Nagarajan, and J. S. Lilley, Nucl. Phys. A **571**, 326 (1994).
[40] J. M. Figueira, J. O. Fernández Niello, A. Arazi, O. A. Capurro, P. Carnelli, L. Fimiani, G. V. Martí, D. Martinez Heimann, A. E. Negri, A. J. Pacheco, J. Lubian, D. S. Monteiro, and P. R. S. Gomes, Phys. Rev. C **81**, 024613 (2010).
[41] A. M. M. Maciel, P. R. S. Gomes, J. Lubian, R. M. Anjos, R. Cabezas, G. M. Santos, C. Muri, S. B. Moraes, R. Liguori Neto, N. Added, N. Carlin Filho, and C. Tenreiro, Phys. Rev. C **59**, 2103 (1999).
[42] J. P. Fernández-García, M. Zadro, A. Di Pietro, P. Figuera, M. Fisichella, O. Goryunov, M. Lattuada, C. Marchetta, A. M. Moro, A. Musumarra, V. Ostashko, M. G. Pellegriti, V. Scuderi, E. Strano, and D. Torresi, Phys. Rev. C **92**, 054602 (2015).
[43] K. O. Pfeiffer, E. Speth, and K. Berthge, Nucl. Phys. A **206**, 545 (1973).
[44] A. Pakou, N. Alamanos, G. Doukelis, A. Gillibert, G. Kalyva, M. Kokkoris, S. Kossionides, A. Lagoyannis, A. Musumarra, C. Papachristodoulou, N. Patronis, G. Perdikakis, D. Pierroutsakou, E. C. Pollacco, and K. Rusek, Phys. Rev. C **69**, 054602 (2004).
[45] A. F. Zeller, D. C. Weisser, T. R. Ophel, and D. F. Hebbard, Nucl. Phys. A **332**, 515 (1979).
[46] P. D. Clark, T. R. Ophel, J. Nurzynski, C. H. Atwood, and D. F. Hebbard, Nucl. Phys. A **352**, 267 (1981).
[47] P. D. Clark, T. R. Ophel, J. S. Eck, A. F. Zeller, J. Nurzynski, D. C. Weisser, and D. F. Hebbard, Nucl. Phys. A **349**, 258 (1980).
[48] H. Kumawat, V. Jha, B. J. Roy, V. V. Parkar, S. Santra, V. Kumar, D. Dutta, P. Shukla, L. M. Pant, A. K. Mohanty, R. K. Choudhury, and S. Kailas, Phys. Rev. C **78**, 044617 (2008).
[49] J. Raynal, Phys. Rev. C **23**, 2571 (1981).
[50] N. Alamanos, Eur. Phys. J. A **56**, 212 (2020).
[51] K. Palli, J. Casal, and A. Pakou, Phys. Rev. C **105**, 064609 (2022).
[52] C. Y. Wong, Phys. Rev. Lett. **31**, 766 (1973).
[53] L. F. Canto, P. R. S. Gomes, J. Lubian, L. C. Chamon, and E. Crema, J. Phys. G **36**, 015109 (2009).
[54] M. Dasgupta, P. R. S. Gomes, D. J. Hinde, S. B. Moraes, R. M. Anjos, A. C. Berriman, R. D. Butt, N. Carlin, J. Lubian, C. R. Morton, J. O. Newton, and A. Szanto de Toledo, Phys. Rev. C **70**, 024606 (2004).
[55] M. Fisichella, A. C. Shotter, P. Figuera, J. Lubian, A. Di Pietro, J. P. Fernandez-Garcia, J. L. Ferreira, M. Lattuada, P. Lotti, A. Musumarra, M. G. Pellegriti, C. Ruiz, V. Scuderi, E. Strano, D. Torresi, and M. Zadro, Phys. Rev. C **95**, 034617 (2017).
[56] C. Beck *et al.*, Phys. Rev. C **67**, 054602 (2003).